

Halogens in hydrothermal sphalerite record origin of ore-forming fluids

Frenzel, M.; Cook, N. J.; Ciobanu, C. L.; Slattery, A.; Wade, B.; Gilbert, S.; Ehrig, K.;
Burisch, M.; Verdugo-Ihl, M. R.; Voudouris, P.;

Originally published:

May 2020

Geology 48(2020)8, 766-770

DOI: <https://doi.org/10.1130/G47087.1>

Perma-Link to Publication Repository of HZDR:

<https://www.hzdr.de/publications/Publ-30705>

Release of the secondary publication
on the basis of the German Copyright Law § 38 Section 4.

1 Halogens in hydrothermal sphalerite record origin of ore-
2 forming fluids

3

4 **Max Frenzel^{1,2,3}, Nigel J. Cook³, Cristiana L. Ciobanu³, Ashley Slattery⁴, Benjamin Wade⁴,**
5 **Sarah Gilber⁴, Kathy Ehrig⁵, Mathias Burisch², Max R. Verdugo-Ihl³, and Panagiotis**
6 **Voudoris⁶**

7

8 *¹Helmholtz-Zentrum Dresden-Rossendorf, Institute Freiberg for Resource Technology,*
9 *Chemnitz Str. 40, 09599 Freiberg, Germany.*

10 *²Chair of Economic Geology and Petrology, Institute of Mineralogy, TU Bergakademie*
11 *Freiberg, Brennhaugasse 14, 09599 Freiberg, Germany.*

12 *³School of Chemical Engineering and Advanced Materials, The University of Adelaide, Adelaide,*
13 *SA 5005, Australia.*

14 *⁴Adelaide Microscopy, The University of Adelaide, Adelaide, SA 5000, Australia.*

15 *⁵BHP Olympic Dam, 55 Grenfell St., Adelaide, SA 5000, Australia*

16 *⁶National and Kapodistrian University of Athens, Faculty of Geology & Geoenvironment, Dept.*
17 *of Mineralogy and Petrology, Panepistimioupolis-Ano Ilisia 15784 Athens, Greece.*

18

19 **ABSTRACT**

20 The halogens Cl and Br are sensitive indicators for the origin of ore-forming fluids. Here, we use
21 a combination of microchemical and microscopic methods to show that measurable
22 concentrations of these elements commonly occur as atomic-scale substitutions within
23 hydrothermal sphalerite. Furthermore, the Cl/Br ratios of the halogen-rich sphalerites
24 investigated in this study are indistinguishable from those of the corresponding ore fluids. Thus,
25 they record fluid compositions, which are in turn closely related to fluid origin. Given the
26 abundance of sphalerite in hydrothermal base-metal deposits, as well as the relative ease of
27 conducting in-situ microchemical analyses, the halogen signature of sphalerite has the potential
28 to become a sensitive proxy to distinguish between different ore-forming environments.

29 .

30 **INTRODUCTION**

31 Due to their ability to form stable complexes with many metals in aqueous solutions,
32 halogens play a key role in mass-transfer processes on Earth and other planetary bodies (Harlov
33 and Aranovich, 2018). Not only are they heavily involved in the formation of most hydrothermal
34 ore deposits (Pirajno, 2018), but they also critically affect the nature and rate of various
35 magmatic and metamorphic processes (Dolejš and Zajacz, 2018; Hammerli and Rubenach,
36 2018).

37 Because they generally behave conservatively during fluid-rock interaction and show
38 distinctive signatures for different crustal reservoirs, Cl and Br have seen extensive use as tracers
39 for the origin of ore-forming hydrothermal fluids (Lecumberri-Sanchez and Bodnar, 2018).
40 While previous studies primarily relied on either the analysis of fluid inclusions or rare silicate
41 minerals such as scapolite to constrain fluid compositions (e.g. Kesler et al., 1995; Hammerli et

42 al., 2013), this article is the first to demonstrate the in-situ measurement of Cl and Br in
43 hydrothermal sphalerite.

44

45

46 **Background**

47 Sphalerite, the cubic polymorph of ZnS, is a common mineral in many types of
48 hydrothermal base-metal deposits. It is well known for its diverse trace element chemistry (Cook
49 et al., 2009; Belissont et al., 2014), recording critical information about the physico-chemical
50 conditions of ore formation (Frenzel et al., 2016). Although high concentrations of Cl in
51 sphalerite have previously been reported (Taylor and Radtke, 1969; Barrie et al., 2009), there is a
52 lack of systematic data on the general prevalence of Cl and other halogens in natural samples, as
53 well as the likely significance and implications of this phenomenon.

54 Because they are not part of the classic suite of chalcophile elements, the halogens are not
55 commonly included in the set of minor and trace elements analyzed in sulfide minerals. This is
56 despite the fact that 1) the Cl⁻ ion is virtually the same size as S²⁻ (Shannon, 1976) and would
57 therefore be expected to readily substitute into sulfide minerals (Blundy and Wood, 2003); and
58 2) Cl/S ratios in hydrothermal fluids are generally high (Yardley, 2005). Of the other halogens,
59 Br⁻ in particular would also be expected to substitute for S²⁻ for similar reasons. These
60 considerations provided the major motivation for this work. As our data shows, halogen
61 substitution into hydrothermal sphalerite may be a common phenomenon, particularly in low-
62 temperature deposits.

63

64

65 MATERIALS AND METHODS

66 To study the occurrence of Cl and Br in natural sphalerite, we selected 12 samples from a
67 diverse range of ore deposits, covering five geological types (Table DR1)¹. Chlorine
68 concentrations were first measured in all samples using electron-probe micro-analysis (EPMA),
69 since this technique offers the best detection limits for Cl. EPMA measurements were
70 supplemented by laser ablation-inductively coupled plasma-mass spectrometry (LA-ICP-MS) to
71 independently verify the occurrence of Cl and determine the abundances of Br and other relevant
72 trace elements (Ga, Ge, In, Co, Tl, Na etc.). Samples with high Cl concentrations were then
73 selected for detailed mapping of Cl distribution by EPMA (μm -scale) and scanning transmission
74 electron microscopy (STEM) coupled with energy-dispersive x-ray spectroscopy (EDX) (nm-
75 scale) to study the spatial distribution of Cl within samples at different scales, and determine its
76 mode of occurrence (substitution or inclusions). Full details of all analytical methods are given in
77 the GSA Data Repository¹ 201Xxxx (Appendix DR1).

78

79 RESULTS

80 EPMA measurements showed that appreciable Cl concentrations occur in three out of the
81 12 investigated samples, ranging from 46 – 4,900 $\mu\text{g/g}$ on average (Table 1). In most samples,
82 however, Cl concentrations were below the detection limit of the EPMA ($\sim 30 \mu\text{g/g}$). Where Cl
83 concentrations exceeded $\sim 100 \mu\text{g/g}$, they were also measurable by LA-ICP-MS and were
84 accompanied by measurable Br and Na concentrations. Laser ablation traces of Cl, Br and Na
85 were generally smooth (Fig. DR1), indicating homogeneous distribution of these elements within
86 the sphalerite matrix at the scale of ablation.

87 Exploratory analysis of the micro-chemical dataset showed that the halogen-rich
88 sphalerites are characterised by significantly higher concentrations of Tl and Ge, and lower Mn
89 concentrations compared to the halogen-poor ones (Appendix DR1). Other trace elements (Cd,
90 Co, Fe, Ga, In etc.) do not show significant correlations with halogen content.

91 Due to their very high halogen contents, the samples from Lisheen (Li-HS-86) and
92 Baisoara (BS7b) were selected for further investigation by EPMA mapping and STEM-EDX
93 imaging. Sample Li-HS-86 is dominated by fine-grained, colour-banded colloform sphalerite,
94 while sample BS7b features more coarsely crystalline black to yellowish-translucent sphalerite.

95 Figure 1 illustrates the results of EPMA mapping for sample Li-HS-86. The
96 corresponding figure for sample BS7b is included in Appendix DR1 (Fig. DR6). In general, the
97 EPMA maps show that:

- 98 1) Cl distribution from the mm- to μm -scale is characterized by complex, sometimes
99 oscillatory, growth zoning qualitatively similar to that shown by the other investigated
100 elements (Cd, Cu, Pb, Fe, where measurable).
- 101 2) In the highest-resolution element maps (step size: 1 μm), Cl is homogeneously distributed
102 within zones of similar composition. There is no evidence for Cl-rich inclusions at this
103 scale.

104 Further examination of Cl-rich areas by high-angle annular dark field (HAADF)-STEM
105 imaging showed that both samples have complex nanostructures featuring nano-scale porosity,
106 inclusions, and sub-grain boundaries (Fig. 2 for Li-HS-86; Fig. DR7 for BS7b). In addition,
107 STEM-EDX-mapping and semi-quantitative analysis allowed for the examination of Cl-
108 distribution at the nano-scale. Here, there are marked differences between the two samples:

- 109 • **Li-HS-86** contains a substantial amount of Pb-Cu-Cl-rich inclusions of unknown
110 speciation that are often associated with porosity. Nevertheless, an appreciable amount of
111 Cl is still homogeneously distributed throughout the material at the investigated scale
112 (~ 1 nm), suggesting it is present as atomic-scale substitutions in the sphalerite (Fig. 2).
113 In fact, a mass balance calculation using LA-ICP-MS data for Cu, Pb and Cl indicates
114 that at least 75% of the total Cl content in Li-HS-86 is hosted as substitutions in the
115 sphalerite rather than as Pb-Cu-Cl-rich inclusions (cf. Appendix DR1).
- 116 • **BS7b** shows no evidence of Cl-rich inclusions, and Cl appears to be homogeneously
117 distributed throughout the material at the investigated scale (~ 1 nm). This suggests it is
118 present exclusively as atomic-scale substitutions in the sphalerite (Fig. DR6).

119 Thus, both samples appear to contain considerable amounts of Cl as homogeneously
120 distributed atomic-scale substitutions in the sphalerite lattice. Unfortunately, the μm - and nm-
121 scale distribution of Br and Na could not be investigated in detail due to their considerably lower
122 concentration levels (rarely exceeding tens of $\mu\text{g/g}$, cf. Table 1), as well as interference from
123 other elements (e.g. Zn on Na). However, no Br- or Na-containing nano-inclusions were found
124 during STEM-EDX work in either of the two samples, suggesting these elements are also present
125 as atomic-scale substitutions.

126

127 **DISCUSSION**

128 Our analytical data strongly suggests that Cl, Br and Na are mostly present in sphalerite
129 as atomic-scale substitutions, rather than solid or fluid inclusions. This observation has several
130 important implications, which we briefly discuss below. Specifically, we consider the likely

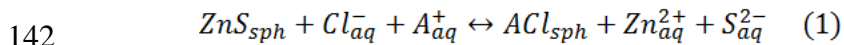
131 substitution mechanisms of the three elements, as well as potential applications to the study of
132 mineral deposits.

133

134 **Substitution mechanisms**

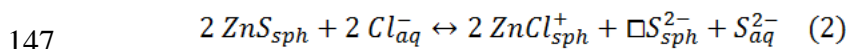
135 Since chloride and bromide ions probably substitute for sulfide ions, their incorporation
136 is expected to introduce a net positive charge on the sphalerite crystal lattice. Therefore, a
137 compensation mechanism is required to maintain charge balance. There are two potential
138 candidates for this mechanism:

139 1) **Coupled substitution**, where the introduction of Cl^- (or Br^-) is accompanied by the
140 exchange of Zn^{2+} for a monovalent cation A^+ (e.g. Cu^+ , Ag^+ , Tl^+ or Na^+) on the zinc
141 sublattice, such that:



143 where the subscripts *aq* and *sph* denote the hydrothermal fluid and the sphalerite solid
144 solution, respectively.

145 2) **Vacancy generation**, where a vacancy is created in the zinc sublattice to compensate for
146 two substituted Cl^- ions:



148 Here, $\square \text{S}_{sph}^{2-}$ denotes a Zn vacancy.

149 Several studies have demonstrated that equivalent compensation mechanisms can explain
150 the substitution of tri- and tetravalent cations for Zn^{2+} , which would otherwise also introduce a
151 net positive charge (e.g. Cook et al., 2012; Cook et al., 2015; Belissont et al., 2016). Comparable
152 mechanisms likely also apply to the incorporation of Na^+ , which would be expected to substitute
153 for Zn^{2+} .

154 To test which mechanism is most likely to be relevant in the investigated samples, we
155 plotted the net negative lattice charge introduced into the sphalerite by mono-, tri- and tetravalent
156 cations against Cl + Br concentrations (Fig. DR5). This showed that approximate charge balance
157 is only maintained in sample BS7b, indicating coupled substitution as the main incorporation
158 mechanism in this sample. In samples Li-HS-86 and TM06.2 on the other hand, there are large
159 imbalances between the net lattice charges introduced by substituting cations and anions,
160 indicating incorporation of Cl⁻ and Br⁻ by Zn-vacancy generation. We note that available
161 XANES data for Ge in TM06.2 (Cook et al., 2015) is also consistent with Zn-vacancy generation
162 as the major charge compensation mechanism in this sample. Thus, incorporation mechanisms
163 vary by sample, with either (1) or (2) more relevant in different cases.

164 While similar charge balance plots as in Fig. DR5 have been used in previous studies to
165 check for the coupled substitution of different cations (e.g. Johan, 1988; Belissont et al., 2014),
166 we note that these studies generally omitted Cl, Br and Na. Given the presence of high Cl
167 concentrations in some sphalerites, the previous conclusions derived from such plots regarding
168 the incorporation mechanisms of Ga, Ge and other tri- and tetravalent ions into the sphalerite
169 lattice may therefore be erroneous and require re-examination in light of our new results.

170

171 **Potential applications**

172 Two major geological applications can be envisaged for measurements of Cl, Br and Na
173 concentrations in sphalerite. First, they may be useful as tracers of fluid origin. Second, it may be
174 possible to use them as indicators for fluid salinity. Together with existing sphalerite
175 geothermometers (Keith et al., 2014; Frenzel et al., 2016), this would enable the characterization
176 of formation temperature, fluid salinity and fluid origin for a sphalerite sample based on only a

177 small set of in-situ microchemical analyses. Given the current need to combine time-consuming
178 microthermometric measurements with at least one other technique (LA-ICP-MS or crush-leach
179 analyses) to yield the same information (Kesler et al., 1995; Seo et al., 2011; Hammerli et al.,
180 2013), this would constitute a substantial step forward.

181 Figure 3 shows that Cl/Br ratios in the investigated sphalerite samples are similar to the
182 ratios of the corresponding ore-fluids. This indicates that no major fractionation occurs between
183 Cl and Br when partitioning from the fluid into the sphalerite, making them suitable as tracers of
184 fluid composition and origin. Agreement between sphalerite and fluid composition is particularly
185 good for samples Li-HS-86 and TM06.2, which show clearly distinct Cl/Br ratios, yet lie within
186 the range expected for their corresponding ore-fluids (Irish-type and MVT fluids). Only in
187 sample BS7b is the Cl/Br ratio somewhat lower than expected for a skarn fluid. However, it still
188 lies within the range covered by the fluid data (incl. outliers). We also note that the skarn dataset
189 available for comparison is extremely limited, deriving from only two ore deposits.

190 Another potential application for Cl, Br and Na in sphalerite is their use as a proxy for
191 fluid salinity. To first order, absolute concentrations of Cl, Br and Na in sphalerite should be
192 controlled by their respective concentrations in the ore-forming fluid (McIntire, 1963). Since
193 NaCl is the major source of salinity in crustal fluids (Yardley, 2005; LeCumberri-Sanchez and
194 Bodnar, 2018), such relationships should be usable in a sphalerite salinometer. However, the fact
195 that high Cl, Br and Na concentrations are only present in low-temperature sphalerites (cf.
196 Appendix DR1) suggests that some temperature control may also exist. A correction for such a
197 dependence would need to be incorporated into any potential salinometer.

198 Overall, the use of element ratios such as Cl/Br shows the greatest potential for direct
199 application in economic geology. Sphalerite salinometry may become feasible in the near future

200 as more analytical data becomes available, allowing for the calibration of Cl and Na
201 concentrations in sphalerite against fluid salinity and potential temperature effects.

202

203 **CONCLUSIONS**

204 To conclude, we have shown that the atomic-scale substitution of Cl and Br for S, and Na
205 for Zn in hydrothermal sphalerite commonly leads to measurable concentrations of all three
206 elements in sphalerite, particularly in base-metal deposits formed at low temperatures (< 200°C).
207 Furthermore, Cl and Br are incorporated without fractionation, such that the Cl/Br ratio in
208 sphalerite records the signature of the ore-forming fluids, in turn allowing for the identification
209 of the fluids' origin.

210 In the future, it may also be possible to infer fluid salinity from absolute Cl and Na
211 concentrations in sphalerite. In combination with existing geothermometers (Keith et al., 2014;
212 Frenzel et al., 2016), this would make the trace-element signature of sphalerite an invaluable
213 indicator in the study of hydrothermal ore deposits. Its major advantages compared to current
214 methods used to determine the temperature, salinity and halogen signature of ore-fluids are the
215 relative ease of sample preparation and analysis compared to fluid inclusion studies, the
216 generally much greater abundance of sphalerite than scapolite in many base-metal deposits, as
217 well as the better control over the geological significance of the sample material compared to
218 crush-leach analyses.

219

220 **ACKNOWLEDGMENTS**

221 We gratefully acknowledge the generous support of the German Academic Exchange
222 Service (DAAD) in funding the senior author's stay at the University of Adelaide where the

223 greatest part of this work was conducted. The geoscientific collections of the TU Bergakademie
224 Freiberg (Dr. Christin Kehrer) are thanked for providing samples from the Tsumeb (TSU) and
225 Freiberg (FG) deposits, while Vedanta Zinc International plc is thanked for allowing access to
226 the Lisheen deposit and the collection of sample Li-HS-86. Last but certainly not least we thank
227 Dr. Jens Gutzmer for fruitful discussions and comments that helped to improve the original
228 version of this manuscript.

229

230 **REFERENCES CITED**

- 231 Barrie, C.D., Boyce, A.J., Boyle, A.P., Williams, P.J., Blake, K., Wilkinson, J.J., Lowther, M.,
232 McDermott, P., and Prior, D.J., 2009, On the growth of colloform textures: a case study
233 of sphalerite from the Galmoy ore body, Ireland: *Journal of the Geological Society of*
234 *London*, v. 166, p. 563-582, <https://doi.org/10.1144/0016-76492008-080>.
- 235 Belissant, R., Boiron, M.-C., Luais, B., and Cathelineau, M., 2014, LA-ICP-MS analyses of
236 minor and trace elements and bulk Ge isotopes in zoned Ge-rich sphalerites from the
237 Noailhac – Saint-Salvy deposit (France): Insights into incorporation mechanisms and ore
238 deposition processes: *Geochimica et Cosmochimica Acta*, v. 126, p. 518-540,
239 <https://doi.org/10.1016/j.gca.2013.10.052>.
- 240 Belissant, R., Munoz, M., Boiron, M.-C., Luais, B., and Mathon, O., 2016, Distribution and
241 oxidation state of Ge, Cu and Fe in sphalerite by μ -XRF and K-edge μ -XANES: insights
242 into Ge incorporation, partitioning and isotopic fractionation: *Geochimica et*
243 *Cosmochimica Acta*, v. 177, p. 298-314, <https://doi.org/10.1016/j.gca.2016.01.001>.

244 Blundy, J., and Wood, B., 2003, Partitioning of trace elements between crystals and melts: Earth
245 and Planetary Science Letters, v. 210, p. 383-397, [https://doi.org/10.1016/S0012-](https://doi.org/10.1016/S0012-821X(03)00129-8)
246 821X(03)00129-8.

247 Cook, N.J., Ciobanu, C.L., Pring, A., Skinner, W., Shimizu, M., Danyushevsky, L., Saini-
248 Eidukat, B., and Melcher, F., 2009, Trace and minor elements in sphalerite: A LA-ICP-
249 MS study: *Geochimica et Cosmochimica Acta*, v. 73, p. 4761-4791,
250 <https://doi.org/10.1016/j.gca.2009.05.045>.

251 Cook, N.J., Ciobanu, C.L., Brugger, J., Etschmann, B., Howard, D.L., de Jonge, M.D., Ryan, C.,
252 and Paterson, D., 2012, Determination of the oxidation state of Cu in substituted Cu-In-
253 Fe-bearing sphalerite via μ -XANES spectroscopy: *American Mineralogist*, v. 97, p. 476-
254 479, <https://doi.org/10.2138/am.2012.4042>.

255 Cook, N.J., Etschmann, B., Ciobanu, C.L., Geraki, K., Howard, D.L., Williams, T., Rae, N.,
256 Pring, A., Chen, G., Johannessen, B., and Brugger, J., 2015, Distribution and substitution
257 mechanism of Ge in a Ge-(Fe)-bearing sphalerite: *Minerals*, v. 2015, p. 117-132,
258 <https://doi.org/10.3390/min5020117>.

259 Dolejš, D., and Zajacz, Z., 2018, Halogens in silicic magmas and their hydrothermal systems, *in*
260 Harlov, D.E., Aranovich, L., eds., *The role of halogens in terrestrial and extraterrestrial*
261 *geochemical processes: Surface, crust, and mantle*, p. 431-544.

262 Frenzel, M., Hirsch, T., and Gutzmer, J., 2016, Gallium, germanium, indium and other minor and
263 trace elements in sphalerite as a function of deposit type – A meta-analysis: *Ore Geology*
264 *Reviews*, v. 76, p. 52-78, <https://doi.org/10.1016/j.oregeorev.2015.12.017>.

265 Hammerli, J., and Rubenach, M., 2018, The role of halogens during regional and contact
266 metamorphism, *in* Harlov, D.E., Aranovich, L., eds., The role of halogens in terrestrial
267 and extraterrestrial geochemical processes: Surface, crust, and mantle, p. 649-712.

268 Hammerli, J., Rusk, B., Spandler, C., Emsbo, P., and Oliver, N.H.S., 2013, In situ quantification
269 of Br and Cl in minerals and fluid inclusions by LA-ICP-MS: A powerful tool to identify
270 fluid sources: *Chemical Geology*, v. 337-338, p. 75-87,
271 <https://doi.org/10.1016/j.chemgeo.2012.12.002>.

272 Harlov, D.E., and Aranovich, L., 2018, The role of halogens in terrestrial and extraterrestrial
273 geochemical processes: surface, crust, and mantle, *in* Harlov, D.E., Aranovich, L., eds.,
274 The role of halogens in terrestrial and extraterrestrial geochemical processes: Surface,
275 crust, and mantle, p. 1-20.

276 Johan, Z., 1988, Indium and germanium in the structure of sphalerite: an example of coupled
277 substitution with copper: *Mineralogy and Petrology*, v. 39, p. 211-229,
278 <https://doi.org/10.1007/BF01163036>.

279 Keith M., Haase, K.M., Schwarz-Schampera, U., Klemd, R., Petersen, S., and Bach, W., 2014,
280 Effects of temperature, sulfur, and oxygen fugacity on the composition of sphalerite from
281 submarine hydrothermal vents: *Geology*, v. 42, p. 699-702,
282 <https://doi.org/10.1130/G35655.1>.

283 Kesler, S.E., Appold, M.S., Martini, A.M., Walter, L.M., Huston, T.J., and Kyle, J.R., 1995, Na-
284 Cl-Br systematics of mineralizing brines in Mississippi Valley-type deposits: *Geology*, v.
285 23, p. 641-644, [https://doi.org/10.1130/0091-](https://doi.org/10.1130/0091-7613(1995)023%3C0641:NCBSOM%3E2.3.CO;2)
286 [7613\(1995\)023%3C0641:NCBSOM%3E2.3.CO;2](https://doi.org/10.1130/0091-7613(1995)023%3C0641:NCBSOM%3E2.3.CO;2).

287 Lecumberri-Sanchez, P., and Bodnar, R.J., 2018, Halogen geochemistry of ore deposits:
288 contributions towards understanding sources and processes, *in* Harlov, D.E., Aranovich,
289 L., eds., The role of halogens in terrestrial and extraterrestrial geochemical processes:
290 Surface, crust, and mantle, p. 261-306.

291 Pirajno, F., 2018, Halogens in hydrothermal fluids and their role in the formation and evolution
292 of hydrothermal mineral systems, *in* Harlov, D.E., Aranovich, L., eds., The role of
293 halogens in terrestrial and extraterrestrial geochemical processes: Surface, crust, and
294 mantle, p. 759-805.

295 Shannon, R.D., 1976, Revised effective ionic radii and systematic studies of interatomic
296 distances in halides and chalcogenides: *Acta Crystallographica*, v. A32, p. 751-767,
297 <https://doi.org/10.1107/S0567739476001551>.

298 Taylor, C.M., and Radtke, A.S., 1969, Micromineralogy of silver-bearing sphalerite from Flat
299 River, Missouri: *Economic Geology*, v. 64, p. 306-318,
300 <https://doi.org/10.2113/gsecongeo.64.3.306>.

301 Yardley, B.W.D., 2005, 100th Anniversary Special Paper: Metal concentrations in crustal fluids
302 and their relationship to ore formation: *Economic Geology*, v. 100, p. 613-632,
303 <https://doi.org/10.2113/gsecongeo.100.4.613>.

304

305 FIGURE CAPTIONS

306 Figure 1. EPMA maps at different scales for sample Li-HS-86 (sph II) showing Cl, Pb and Cu
307 distribution, superimposed on high-contrast BSE images of the polished sample surface: A) mm-
308 scale distribution, B) intermediate scale, C) micron-scale.

309

310 Figure 2. Summary of STEM and STEM-EDX imaging in sample Li-HS-86 (sph II): A)
311 overview of sample foil with corresponding SAED pattern in lower left-hand corner; B) and C)
312 detailed HAADF-STEM images of A) as indicated; D) detail of B) showing close-up of nano-
313 porosity; E) detail of C) showing inclusions; F) detail of E) showing close-up of inclusion hosted
314 in nano-pore; G) detail of C) and EDX maps of same area; H), I) and J) summed EDX spectrum
315 for different parts of the map area shown in G) as indicated (grey line – data, red line – fitted
316 spectrum, green line – fitted background). Note complex nanostructure of the material (different
317 domains, pores, bright inclusions) and high Cl contents hosted in bright inclusions as well as
318 sphalerite matrix.

319

320 Figure 3. Comparison of Cl/Br ratios in halogen-rich sphalerite samples from this study with
321 literature data on relevant ore-forming and crustal fluids (see Appendix DR4 for complete fluid
322 dataset including a reference list).

323

324 ¹GSA Data Repository item 201Xxxx, including Appendixes DR1 (detailed methods and
325 summary of analytical results), DR2 (full EPMA dataset), DR3 (full LA-ICP-MS dataset) and
326 DR4 (fluid database used for Fig. 3), is available online at

327 www.geosociety.org/pubs/ft20XX.htm, or on request from editing@geosociety.org.